

Supporting Information

Why surface hydrophobicity promotes CO₂ electroreduction: a case study of hydrophobic polymer N-heterocyclic carbenes

Qiang Luo,¹ Hanyi Duan,² Michael C. McLaughlin,¹ Kecheng Wei,³ Joseph Tapia,⁴ Joseph A. Adewuyi,¹ Seth Shuster,¹ Maham Liaqat,¹ Steven L Suib,¹ Gaël Ung,¹ Peng Bai,^{*,4} Shouheng Sun^{*,3} and Jie He^{*,1,2}

¹Department of Chemistry, and ²Polymer Program, Institute of Materials Science, University of Connecticut, Storrs, CT 06269, United States.

³Department of Chemistry, Brown University, Providence, Rhode Island 02912, United States.

⁴Department of Chemical Engineering, University of Massachusetts, Amherst, Massachusetts 01003, United States.

Email: jie.he@uconn.edu (JH), shouheng_sun@brown.edu (SS) and pengbai@umass.edu (PB)

Contents

1. Chemicals and materials
2. Synthesis of poly(ethylene oxide) (PEO) imidazolium (P1)
3. Synthesis of polystyrene (PS) imidazolium (P2)
4. Synthesis of block copolymer of PEO-*b*-PS imidazolium (P3) and PEO-*b*-PS-SH
5. Synthesis of 1-butyl-3-methyl-1H-benzimidazolium bromide (BMB-Im)
6. Synthesis of citrate-capped AuNPs and Au/C
7. Surface ligands modifications of AuNPs with various polymers
8. *In-situ* SEIRAS electrode preparation
9. Electrochemical measurements
10. *In-situ* ATR-SEIRAS measurements
11. Determination of diffusion coefficients of molecular probes
12. Determination of grafting density
13. Other characterizations
14. Molecular dynamics simulations

Figure Contents

Supporting Figure S1. NMR spectra and synthetic route of P1.

Supporting Figure S2. NMR spectra and synthetic route of P2.

Supporting Figure S3. NMR spectra and synthetic route of P3.

Supporting Figure S4. NMR spectra data of molecular NHC BMB-Im.

Supporting Figure S5. FT-IR spectra of pure ligands P1, P2, P3, BMB-Im and Au NPs modified by P1, P2, P3 and BMB-Im.

Supporting Figure S6. XPS spectra of BMB-Im modified Au/C samples.

Supporting Figure S7. TGA thermograms of individual P1, P2, P3, Au samples and functionalized Au NPs with P1, P2 and P3.

Supporting Figure S8 CV curves of Au-P1 and Au-P3 under different atmosphere and LSV curves of Au-P1 and Au-BMB-Im.

Supporting Figure S9. In-situ ATR-SEIRAS spectra of Au modified with ligands of P1 and BMB-Im.

Supporting Figure S10. CV curves of Au NPs and various ligands of P1, P2, P3 modified Au NPs with the presence of $K_3Fe(CN)_6$.

Supporting Figure S11. CV curves of Au NPs and various ligands of P1, P2, P3 modified Au NPs with the presence of $Ru(NH_3)_6Cl_3$.

Supporting Figure S12. CV curves of Au NPs and various ligands of P1, P2, P3 modified Au NPs with the presence of Fc-COOH.

Supporting Figure S13. EIS measurements of Au NPs and various ligands of P1, P2, P3 modified Au NPs.

Supporting Figure S14. Molecular dynamics (MD) simulations with various CO_2 concentration.

Supporting Figure S15. Additional TEM images of Au NPs and AuNPs capped with P3.

Supporting Table S1. The average faradic efficiency and kinetic current density analysis of pure Au NPs.

Supporting Table S2. The average faradic efficiency and kinetic current density analysis of Au NPs modified with P1.

Supporting Table S3. The average faradic efficiency and kinetic current density analysis of Au NPs modified with P2.

Supporting Table S4. The average faradic efficiency and kinetic current density analysis of Au NPs modified with P3.

1. Chemicals and materials

Anisole (anhydrous, 99.7%), α -bromoisobutyl bromide (BBiB, $\geq 98\%$), N,N' -dicyclohexylcarbodiimide (DCC), styrene, ethyl α -bromoisobutyrate (EBiB) ($\geq 98\%$), copper bromide (Cu(I)Br, 99.999%), poly(ethylene oxide) monomethyl ether (PEO₄₄-OH, $M_n=2000$ g/mol), N,N,N',N'',N''' -pentamethyldiethylenetriamine (PMDETA), ethyl α -bromoisobutyrate (EBiB, 98%), gold(III) chloride trihydrate (HAuCl₄·3H₂O), azobisisobutyronitrile (AIBN, 98%), 4-Dimethylaminopyridine (DMAP, 98%), sodium citrate, potassium bicarbonate (KHCO₃), N,N -dimethylformamide (DMF), tetrahydrofuran (THF), chloroform, dichloromethane (DCM), ethanol (anhydrous, $\geq 99.5\%$), *n*-hexane, 1-methylbenzimidazole (99%) were purchased from Sigma Aldrich. Styrene was passed through a basic aluminum oxide column prior to use for the removal of inhibitors. Printex U activated carbon was kindly gifted from Orion. Deionized water (High-Q, Inc. 103S Stills) with a resistivity of >10.0 M Ω was used in all experiments.

2. Synthesis of poly(ethylene oxide) (PEO) imidazolium (P1)

PEO₄₄-Br was synthesized by the DCC coupling reaction between PEO₄₄-OH and 4-bromobutyric acid. In a typical synthesis, PEO₄₄-OH (15 g, 7.5 mmol, 1 eq), 3-bromopropionic acid (2.3 g, 15 mmol, 2 eq), DCC (3.09 g, 15 mmol, 2 eq) and 4-dimethylaminopyridine (36 mg, 0.29 mmol) were dissolved into 60 mL of anhydrous DCM. The flask was purged with dry nitrogen for 15 min. The reaction was allowed to run at room temperature for 48 h. Then the mixture was diluted with 140 mL of DCM and washed with saturated NaHCO₃, diluted HCl solution (pH 4) and saturated NaCl aqueous solution sequentially. The obtained polymer solution was dried over Na₂SO₄ and concentrated using rotatory evaporator after passing a short silica gel column, which was then purified by precipitating into cold diethyl ether three times. Secondly, the halide end PEO₄₄-Br was converted through alkylation with 1-methylbenzimidazole. Specifically, PEO₄₄-Br (5.0 g, 2.5 mmol), 1-methylbenzimidazole (1.32 g, 10 mmol) and trace KI (10 mg, 0.06 mmol) were mixed in 25 mL of DMF. The whole reaction system was then transferred into an oil bath for continuing reaction at 95 °C for 24 h after purging N₂. Excess 1-methylbenzimidazole was removed by dialyzing against ethanol for 3 days. The powder of PEO₄₄-Im was obtained by evaporating solvent and precipitating in diethyl ether. Lastly, an anion exchange of PEO₄₄-Im was carried out. Typically, 0.5 mmol of PEO₄₄-Im (1 g) and 2 mmol of KHCO₃ (200 mg) were added into 20 mL of THF. The mixture was stirred for two days at room temperature after purging with N₂ for 5 min. Then, the reaction was cooled down with an ice bath to remove KBr. The polymer PEO₄₄-Br (P1) was then purified and collected in DCM after passing through a short silica column removing excess KBr salt and precipitating in diethyl ether.

3. Synthesis of polystyrene (PS) imidazolium (P2)

PS₁₀₀-Br was synthesized through atom transfer radical polymerization (ATRP) using ethyl α -bromoisobutyrate (EBiB) as an initiator for reaction. Typically, styrene (10 g, 96.15 mmol, 120 eq) and Cu(I)Br (173 mg, 1.2 mmol, 1.5 eq) were mixed with 10 mL of anisole in a 50 mL flask. After purging with N₂ for 5 min, PMDETA (276.8 mg, 1.6 mmol, 2 eq) was injected into the above solution, followed by three times of freeze-pump-thaw. EBiB (156 mg, 0.8 mmol, 1 eq) was added into the reaction system and continued to purge with N₂ for another 15 min. After polymerization at 90 °C for 12 h, the reaction was cooled down to room temperature. Then, 10 mL of DCM was added to dilute the polymer solution. The mixture was passed through a silica gel column to remove the catalysts until clear and colorless eluents were obtained. After concentrating the solution with a rotary evaporator, the product was collected through precipitation with methanol three times and dried under vacuum. The numbers of repeat units of styrene were calculated to be 100 through end-group analysis using the ¹H NMR peak at 4.4 ppm of the -CH- end group directly connected with Br atom in PS-Br. The obtained polymer has a M_n of 10.7 kg mol⁻¹ and \bar{D} of 1.14, measured from GPC calibrated by monodispersed PS.

PS₁₀₀-Im was synthesized by the quaternization reaction between PS-Br and 1-methylbenzimidazole. PS₁₀₀-Br (2 g, 0.19 mmol) 1-methylbenzimidazole (528 mg, 4 mmol) and trace KI (10 mg, 0.06 mmol) were mixed in 25 mL of DMF. After purging N₂ for 15 min, the reaction was carried out at 95 °C for 24 h. The PS-Im was purified by precipitating into ethanol three times and dried under vacuum. 1 g of purified PS-Im (0.095 mmol) and 100 mg KHCO₃ (1 mmol) were mixed in 20 mL THF, and the mixture was stirred at room temperature for 48 h after purging N₂. Afterwards, the reaction was cooled down with an ice bath. The column procedure was repeated twice to remove salts. The final product was obtained by precipitation into ethanol twice and dried under vacuum.

4. Synthesis of the BCP of PEO-*b*-PS imidazolium (P3)

The ATRP initiator PEO₄₄-Br was synthesized using a previously reported method.¹ Briefly, PEO₄₄-OH (10 g, 5 mmol, 1 eq), triethylamine (1g, 10 mmol, 2 eq) and trace amount of 4-dimethylaminopyridine (DMAP, 10 mg) were dissolved into 60 mL of anhydrous DCM. The solution was cooled by an ice-bath and purged N₂ for 10 min. Then, α -bromoisobutyl bromide (2.3 g, 10 mmol, 2 eq) dissolved into 5 mL of anhydrous DCM, was added dropwise to the polymer solution under N₂. The mixture was stirred under room temperature for 36 h then diluted by DCM. The polymer solution was washed with saturated NaHCO₃, diluted HCl solution (pH=4) and saturated NaCl aqueous solution sequentially. The prepared PEO₄₄ ATRP initiator was obtained by precipitation using cold diethyl ether.

Styrene (9.35 g, 90 mmol, 300 eq), Cu(I)Br (65 mg, 0.45 mmol, 1.5 eq), PEO₄₄-Br initiator (0.6 g, 0.3 mmol, 1 eq) and 30 mL of anisole were added into a 100 mL Schlenk flask. In order to remove dissolved O₂, three times of freeze-pump-thaw procedures were conducted by using liquid nitrogen. During the last time, PMDETA ligand (104 mg, 0.6 mmol, 2 eq) was quickly added into the Schlenk flask, which was sealed after filling with nitrogen. The ATRP process of styrene was carried out at 90 °C for 12 h. Afterwards, 30 mL of DCM was added to quench the polymerization followed by cooling down to room temperature. A short silica gel column was used to remove the copper catalyst. The column was repeated until the eluents were totally clear, indicating there was no copper salts residual left. The synthesized BCP was obtained after precipitation with cooled n-hexane three times and dried under vacuum. The molecular weight and dispersity index of the block copolymer is 27.0 kg/mol and 1.18 based on NMR spectrum and gel permeation chromatography (GPC) calibrated by monodispersed polystyrene, respectively.

Afterwards, PEO₄₄-*b*-PS₂₃₀-Br (5 g, 0.19 mmol), 1-methylbenzimidazole (649 mg, 4.9 mmol) and trace KI (10 mg, 0.06 mmol) were mixed in 25 mL of DMF. After purging N₂ for 15 min, the solution was transferred into an oil bath and the reaction was carried out at 95 °C for 24 h. Consequently, the PEO₄₄-*b*-PS₂₃₀-Im product was purified by precipitating from ethanol three times and dried under vacuum.

For the anion exchange process, 1 mmol of KHCO₃ (100.6 mg) and 0.019 mmol of PEO₄₄-*b*-PS₂₃₀-Im (500 mg) were mixed with 10 mL of dry THF. After purging with N₂ for 10 min, the mixture was carried out and kept stirring at room temperature for 48 h. Afterwards, the reaction was cooled down with an ice bath. To ensure the lowest residual potassium salts, the column procedure was repeated twice. The final product of PEO₄₄-*b*-PS₂₃₀-Im (P3) was obtained by precipitate into ethanol twice and dried under vacuum.

PEO₄₅-*b*-PS₂₆₇-SH was synthesized using our previously reported method.²

5. Synthesis of 1-butyl-3-methyl-1H-benzimidazolium bromide (BMB-Im)

To a round bottom flask was added N-methyl benzoimidazole (0.556 mmol) and 1-bromobutane (0.06 mL, 0.556 mmol). Then 5 mL of acetonitrile was added to the flask. The reaction was stirred at 85 °C overnight. The solvent was evaporated in vacuo to obtain a sticky solid. The solid was washed several times with hexane to remove unreacted starting material. After purification, a white powdery solid was obtained. Yield = 30%. ¹H NMR (400 MHz, CDCl₃): δ (ppm): 11.63 (s, 1H), 7.73 (broad, 4H), 4.61 (t, 2H), 4.34 (s, 3H), 2.06 (m, 2H), 1.50 (m, 2H), 1.01 (t, 3H).

6. Synthesis of citrate capped AuNPs and Au/C

6.1 AuNPs

Citrate-capped Au NPs (diameter 14±1.7 nm) were synthesized through the method report previously.³ Typically, 100 mg of HAuCl₄ precursor was added into 500 mL of H₂O following by heating up to 100 °C with stirring. Afterwards, 30 mL of sodium citrate (1 wt%) was quickly injected into the above solution. The solution was stirred for another 30 min before cooling down to room temperature and ready for use without further purification.

6.2 Au/C

AuNPs loaded on carbon were synthesized by mixing activated carbon (Printex U, 50 nm) with as-synthesized AuNPs. Briefly, Au/C catalyst with a loading amount of 40 wt% AuNPs was obtained by mixing the stock solution of AuNPs with the activated carbon (Printex U). Typically, 30 mg of carbon was firstly dispersed into 10 mL of ethanol by sonicated for 30 min. Then, the above solution was mixed with 120 mL of the Au stock solution (0.1 mg mL⁻¹) further under the sonication for another 30 min. After stirring overnight, Au/C was collected by centrifugation and dried under vacuum.

7. Surface ligands modifications of AuNPs with various polymers

2 mL of polymer solution (5 mg mL⁻¹) in methanol was added into 5 mL of a methanol solution containing 5 mg of Au/C (40 wt%) under stirring at room temperature and let it react for overnight. Then, the modified Au /C was collected and purified by methanol three times. The powder was finally obtained by drying under vacuum. The surface modification of P1-P3 and PEO-*b*-PS-SH was done with a similar procedure. The modification of Au/C with BMB-Im was carried out in aqueous solution containing 0.1 M of NaHCO₃.

8. *In-situ* SEIRAS electrode preparation

For the cathode preparation, a commercial 60° Si ATR crystal (Pike Technologies) was mechanically polished with alumina suspensions of 1.0, 0.3, and 0.05 μm (Buehler) with microcloth pads attached to a glass slide. Consequently, to remove any silica residual the Si crystal surface was sonicated in water and then acetone three times followed by drying under N₂ flow. Then, in order to remove any surface organic contaminations, the Si prism was immersed in piranha solution, specifically, 3:1 by volume solution H₂SO₄ (95–98 wt.%) and H₂O₂ (30 wt.%) for 20 min. Then, the reflecting side of the Si prism was immersed in NH₄F (40 wt.%) continuously for 2 min to improve the adhesion of Au film growing following rinsed with DI water. The method used here was based on previous report with modifications.⁴ Typically, the Si surface was immersed in 1:4.4 by volume mixture of HF (2 wt.%) and Au plating solution. Specifically, the Au plating solution composed of two solutions: a) 0.03 M HAuCl₄·3H₂O, 0.026 M NaOH b) 0.3 M Na₂SO₃ + 0.1 M Na₂S₂O₃ + 0.1 M NH₄Cl. During the electroless deposition of Au nanostructured film, the Si crystal (22 mm diameter) was partially soaked into the plating solution preheated to 55 °C and left for 3 min giving out a vibrant Au metal colored film. Afterwards, the Si prism was quenched with DI water removing any plating solution residual before measurement.

9. Electrochemical measurements

The electrochemical experiments were carried out through a CH Instrument 627E Potentiostat. A pyrolytic graphite (PG) electrode loaded with catalysts ink was used as a working electrode, together with a saturated calomel electrode (SCE) as a reference electrode and a carbon rod as a counter electrode. All potentials presented in this manuscript were converted to reversible hydrogen electrode (RHE) through $E_{\text{RHE}} = E_{\text{SCE}} + 0.244 \text{ V} + 0.0591 \times \text{pH}$. For the catalyst preparation, the ink containing 5 mg of the catalyst, 1000 μL of H₂O and 200 μL of isopropanol was sonicated for 30 min. 10 μL of the catalyst ink was then dropped on a PG electrode and dried thoroughly under N₂ before using. Electrochemical active surface area (ECSA) characterization of catalysts was carried out in N₂-saturated 0.5 M H₂SO₄ solution at a scan rate of 100 mV s⁻¹. All ECSAs of different Au catalysts were calculated using the reverse reduction peaks of surface monolayer AuO compound. The reference charge (C₀) value of Au used here was 390 μC·cm⁻² for real surface area calculation.⁵ All electrochemical CO₂ reduction measurements of different Au/C catalysts were conducted in a customized H-cell with a Nafion membrane (Nafion 117) separating cathode and anode counterpart of the whole reaction cell. Specifically, one side of the H-cell consists of a PG work electrode and SCE reference electrode, while the other side consists of carbon rod as counter electrode. Each side of the H-cell cylinder was refilled with 27 mL of KHCO₃ (0.1 M) electrolyte and 11 mL headspace left. To have CO₂-saturated electrolyte, CO₂ was continuously purged for 30 min. Linear sweep voltammetry (LSV) scans were performed in 0.1 M KHCO₃ solution in the potential range of -0.16 to -1.16 V at a scan rate of 10 mV s⁻¹. Gas products were analyzed using gas chromatography (GC). The chronoamperometry (i-t) was executed at different potentials to evaluate the product and stability of catalysts. To study the size and morphology evolutions of AuNPs, catalysts with various periods of electrolysis were collected through sonication. Afterwards, the catalysts were dispersed in ethanol followed sonicated for another 1 min before using for TEM imaging characterization.

10. In-situ ATR-SEIRAS measurements

All SEIRAS experiments were carried out using a customized Teflon single-chamber electrochemical cell mounted on IR beam. The Teflon electrochemical cell was accommodated onto the Si prism with the Au film, carbon rod and SCE as working electrode, counter electrode and reference electrode, respectively. In addition, to remove moisture in surrounding environment, N₂ was purged into all the attachment and the surrounding chambers overnight before the start of the experiment. Before using as working electrode, the deposited Au film surface needs to be activated by using cyclic voltammetry (CV) scans at 50 mV s⁻¹ in 0.1 M KHCO₃ until it became stable. The background scan of the single-beam spectrum was taken during electrocatalysis before each measurement in absorbance unit (a.u.). The ATR-SEIRAS measurements were conducted on a Nicolet iS50 FTIR Spectrometer coupled with the Pike Technologies VeeMAX III ATR accessory and liquid nitrogen-cooled MCT detector. All spectra were collected with a 4 cm⁻¹ resolution and 16 scans. Spectra are presented in absorbance where positive and negative peaks signify an increase and decrease in the corresponding interfacial ligands and species, respectively. All potentials are given on the reversible hydrogen electrode (RHE) scale unless noted otherwise.

11. Estimation of diffusion coefficients of ligands-modified electrodes

All electrochemical measurements towards dynamic molecular transport upon catalysts interface were carried out in a three-electrode single cell at room temperature. A saturated calomel electrode (SCE) and a carbon rod were used as reference and counter electrode, respectively. All tests were recorded with the presence of three molecular probes including K₃Fe(CN)₆, Ru(NH₃)₆Cl₃ and Fc-COOH with certain amount. For all catalysts, CVs were collected with different scan rate in the range of 40 to 100 mV/s. Randles-Ševčík equation was used to calculate diffusion coefficients as shown below.⁶

$$i_p = 0.4463nFAC_o \left(\frac{nFvD_o}{RT} \right)^{\frac{1}{2}}$$

where F is the Faraday's constant, A is the electrode surface area, R is the gas constant, T is the temperature, n is the number of electrons during redox reaction. For the Au/C samples with K₃Fe(CN)₆,

$$\begin{aligned} i_p &= (2.69 \times 10^5) n^{\frac{3}{2}} A D_o^{\frac{1}{2}} C_o v^{\frac{1}{2}} \\ D_o &= \left(\frac{i_p}{(2.69 \times 10^5) n^{\frac{3}{2}} A C_o v^{\frac{1}{2}}} \right)^2 \\ &= \left(\frac{0.00355}{(2.69 \times 10^5) \times 1^{\frac{3}{2}} \times 0.1963 \times 5 \times 10^{-5}} \right)^2 \\ &= 1.81 \times 10^{-6} \text{ cm}^2 \text{ s}^{-1} \end{aligned}$$

Similarly, to calculate the diffusion coefficients of P1-Au/C, P2-Au/C and P3-Au/C with K₃Fe(CN)₆, the same process were carried out only with different peak current. Thus, the diffusion coefficients of P1-Au/C $D_o =$

$$\left(\frac{0.00262}{(2.69 \times 10^5) \times 1^{\frac{3}{2}} \times 0.1963 \times 5 \times 10^{-5}} \right)^2 = 0.98 \times 10^{-6} \text{ cm}^2 \text{ s}^{-1}; \text{ P2-Au/C } D_o = \left(\frac{0.00264}{(2.69 \times 10^5) \times 1^{\frac{3}{2}} \times 0.1963 \times 5 \times 10^{-5}} \right)^2 = 1.00 \times 10^{-6} \text{ cm}^2 \text{ s}^{-1}; \text{ P3-Au/C } D_o = \left(\frac{0.00298}{(2.69 \times 10^5) \times 1^{\frac{3}{2}} \times 0.1963 \times 5 \times 10^{-5}} \right)^2 = 1.27 \times 10^{-6} \text{ cm}^2 \text{ s}^{-1}.$$

The standard deviations are obtained based on independent three times measurements. For the diffusion coefficients based on Ru(NH₃)₆Cl₃ and Fc-COOH probes, the same calculation processes were carried out and standard deviations were obtained through independent three times measurements.

Electrochemical impedance spectroscopy (EIS) was carried out in a three-electrode cell. A D_{CO_2} obtained from this technique could be used to analyze and compare Au NPs modified with different ligands, giving out different local microenvironment toward CO₂ electroreduction. CO₂ saturated 0.1M KHCO₃ served as electrolyte during all measurements. EIS was recorded from 100 kHz to 1 Hz at -0.8V vs RHE. Diffusion coefficients of CO₂ were calculated shown as below.⁷

$$D = \frac{R^2 T^2}{2(A n^2 F^2 C \sigma)^2}$$

where R present the gas constant ($8.314 \text{ J K}^{-1} \text{ mol}^{-1}$), T is the reaction temperature (298 K), n is the number of electrons during electrocatalysis, F is the Faraday's constant, A is the surface area, ω is the angular frequency, C is the concentration of dissolved CO_2 , and σ is the Warburg factor, related to the Z' . For the Au/C samples,

$$D = \frac{8.314^2 \times 298^2}{2 \times (10.13 \times 2^2 \times 96485.33^2 \times 1.58 \times 10^{-7} \times 1262.08)^2} = 5.43 \times 10^{-10} \text{ cm}^2 \text{ s}^{-1}$$

Similarly, for the P1-Au/C, P2-Au/C and P3-Au/C, the EIS were carried out at same conditions with using Warburg facto of 1903.90, 1369.36 and 1530.24, respectively. So, the D_{CO_2} of P1 on Au $D =$

$$\frac{8.314^2 \times 298^2}{2 \times (9.24 \times 2^2 \times 96485.33^2 \times 1.58 \times 10^{-7} \times 1903.90)^2} = 2.87 \times 10^{-10} \text{ cm}^2 \text{ s}^{-1}; \text{ the } D_{\text{CO}_2} \text{ of P2 on Au } D =$$

$$\frac{8.314^2 \times 298^2}{2 \times (5.72 \times 2^2 \times 96485.33^2 \times 1.58 \times 10^{-7} \times 1369.36)^2} = 1.44 \times 10^{-9} \text{ cm}^2 \text{ s}^{-1}; \text{ the the } D_{\text{CO}_2} \text{ of P3 on Au } D =$$

$$\frac{8.314^2 \times 298^2}{2 \times (5.13 \times 2^2 \times 96485.33^2 \times 1.58 \times 10^{-7} \times 1530.24)^2} = 1.44 \times 10^{-9} \text{ cm}^2 \text{ s}^{-1}.$$

12. Determination of polymer grafting density

The grafting density of ligands each AuNPs was calculated from thermogravimetric analysis (TGA) analysis. The equation was shown as below.

$$\text{polymer chains / NPs} = \frac{\text{the total number of polymer chains}}{\text{the total surface area of Au NPs}}$$

$$\text{the total number of polymer chains} = \frac{m_{\text{polymer}}}{M_{\text{polymer}} \times N_A}$$

$$\text{the total surface area of Au NPs} = S_{\text{NP}} \times \frac{\frac{m_{\text{Au}}}{M_{\text{Au}}}}{\rho_{\text{Au}} \times \frac{V_{\text{NP}}}{M_{\text{Au}}}}$$

where, the m_{polymer} and m_{Au} refers to the mass of polymer ligands and AuNPs, respectively. M_{polymer} and M_{Au} are molecular weight of polymer ligands and Au atoms, respectively. N_A is the Avogadro constant. ρ_{Au} is the density of bulk Au materials. S_{NP} and V_{NP} refer to the surface area and volume of an individual AuNP.

Taking Au-P1/C catalysts as an example, the calculation details are as followings. As shown in TGA from TGA analysis, the weight loss of 98.4 wt% was recorded from the thermal decomposition of P1 at 700 °C relative to the initial mass. To calculate the grafting density of ligand P1 on Au/C, 5.53 mg of Au-P1/C was used for the TGA experiments. Unmodified Au/C was used as the blank sample to deduce the background showing a weight loss of 4.4 wt%. The weight loss of Au-P1/C sample was 8.0 wt% at 700 °C. Afterwards, the weight ratio of P1 could be obtained, $(8 \text{ wt}\% - 4.4 \text{ wt}\%) / 98.4 \text{ wt}\% = 3.66 \text{ wt}\%$. Based on the amount of loading catalysts, the grafting mass could be calculated, $5.525 \text{ mg} \times 3.66 \% = 0.20 \text{ mg}$. Then, the grafting density could be calculated from,

$$\text{total number of polymer chains} = \frac{m_p}{M_p} \times N_A = \frac{0.202 \text{ mg}}{2218.1 \text{ g mol}^{-1}} \times 6.022 \times 10^{23} = 5.49 \times 10^{16}$$

$$\text{total number of Au NP} = \frac{\frac{m_{\text{Au}}}{M_{\text{Au}}}}{\rho_{\text{Au}} \times \frac{V_{\text{NP}}}{M_{\text{Au}}}} = \frac{\frac{2.13 \text{ mg}}{196 \text{ g mol}^{-1}}}{19.3 \text{ g cm}^{-3} \times \frac{1.436 \times 10^{-24} \text{ m}^3}{196 \text{ g mol}^{-1}}} = 7.68 \times 10^{13}$$

$$\text{surface area of Au NP} = 4\pi r_{\text{Au}}^2 = 4 \times 3.14 \times (7 \times 10^{-9})^2 = 615 \text{ nm}^2$$

$$\text{Finally, the grafting density of P1 could be calculated } \frac{5.49 \times 10^{16}}{615 \text{ nm}^2 \times 7.68 \times 10^{13}} = 1.16 \text{ chains/nm}^2$$

Similarly, to determine the grafting density of P2 on Au, 3.70 mg of Au-P2/C was employed for TGA experiments. Two TGA experiments were carried out for unmodified Au/C and Au-P2. Unmodified Au/C was also used as the blank to deduce the background, which shows a loss weight of 4.4 wt%. The weight loss of Au-P2 is 14.9 wt% at 700 °C. This gives the weight ratio of P2, $(14.9 \text{ wt}\% - 4.4 \text{ wt}\%) / 96.9 \text{ wt}\% = 10.8 \text{ wt}\%$. Using the initial loading amount of Au-P2/C for TGA examination, the grafting mass of P2 on Au-P2 is 0.40 mg. Consequently, the number

of polymer chain and Au NP were 2.26×10^{16} and 4.76×10^{13} , respectively. Using the same equation, the grafting density of P2 was 0.77 chains/nm².

For grafting density of P3 on Au, 3.6 mg of Au-P2/C was used. The weight loss of Au-P3 is 22.7 wt% at 700 °C. This gives the weight ratio of P3, (22.7 wt% 4.4 wt%)/97.6 wt% =18.8 wt%. Afterwards, the grafting mass of P3 on Au-P3 is 0.67 mg. Similarly, the number of polymer chain and Au NP were 1.50×10^{16} and 4.20×10^{13} , respectively. Finally, the grafting density of P3 was 0.58 chains/nm².

13. Other characterizations

Thermogravimetric analysis (TGA) was performed in the atmosphere of N₂ in the temperature range from 100 °C to 700 °C at a heating rate of 10 °C through TA Instrument TGA Q-500 facility. Before TGA data collection, the samples were incubated at 100 °C for 1h under N₂ to remove any solvent residual. Fourier transform infrared spectroscopy (FT-IR) was collected using a Alpha FT-IR Spectrometer Bruker. The transmission electron microscopy (TEM) was recorded using a FEI Tecnai 12 G2 Spirit BioTWIN. TEM samples were dropped casted onto a carbon-based copper grid with 400 mesh. X-ray photoelectron spectroscopy (XPS) results were collected performed on a ThermoFisher K-Alpha XPS spectrometer with an Al K α source ($\lambda = 1486.6$ eV) radiation source, pass energy of 25 eV and step size of 0.1 eV. All XPS spectra collected here were processed and analyzed using CasaXPS software. (version 2.3.12) and corrected with a C 1s BE value of 284.6 eV. ¹H NMR spectra of liquid samples were performed on a Bruker Avance 400 MHz spectrometer. The size exclusion chromatography (SEC) examinations were carried out using a Waters SEC-1 (1515 HPLC pump and Waters 717 Plus auto injector) equipped with a Varian 380-LC evaporative light scattering detector and three Jordi Gel fluorinated DVB columns (1-100K, 2-10K, and 1-500 Å). The tetrahydrofuran (THF) was used as elution solvent at the flow rate of 1.25 mL/min, while the data were processed using Empower SEC software (Waters, Inc.).

14. Molecular dynamics simulations

MD simulations were performed using the LAMMPS software⁸, version 8Feb2023, to understand the solvation environment of Au-P2 nanoparticles in contact with aqueous CO₂ solutions of varying concentrations. The temperature was maintained at T = 300 K using the Nose-Hoover thermostat with a time constant of 100 fs. The polymer chains were modeled using the TraPPE force field⁹⁻¹² for all non-bonded parameters, angle bending, backbone dihedrals, and other equilibrium geometries and AMBER86^{13, 14} for the force constants for bond stretching and aromatic ring dihedrals. For gold atoms, non-bonded parameters were taken from UFF¹⁵ and bonded parameters with tethered polymers were taken from Nayis et al.¹⁶ Water was described using the TIP4P model¹⁷ with the SHAKE¹⁸ algorithm to keep a rigid geometry. CO₂ was modeled using the TraPPE forcefield¹⁹ with stretching and bending constants set to 5000 kcal/mol/Å² and 500 kcal/mol/deg² to keep them relatively rigid. Partial charges for the benzene rings and NHC were calculated using CM5 charge model.²⁰ Non-bonded interactions between unlike atoms were calculated with the Lorentz-Berthelot combining rules. Lennard-Jones interactions were evaluated to a spherical cut-off of 1.4 nm and Coulomb interactions were calculated using the particle-particle-particle-mesh (PPPM) method with a relative error in forces of 10⁻⁴ kcal/mol/Å.

Au was represented by a 1.1 nm thick slab, which consists of 864 atoms and exposes the (111) surface. The PS chains consist of an imidazole head, 66 syndiotactic styrene repeating units, and a methyl tail. Nine polymer chains were attached to the gold surface to reach a density of 0.89 chains/nm². A short MD run was performed before the entire system was immersed into an equilibrated water box. Any water molecules that overlapped with the polymers or the AuNP were removed, resulting in a combined system of size 3.4608 × 3.4608 × 20 nm³ and 3004 water molecules. The merged system was further equilibrated in the NVT ensemble for 400 ps, after which one or two CO₂ molecules were incorporated into the system by replacing the same number of water molecules. Six different configurations were created at each CO₂ concentration with CO₂ located at z = 5.6 to 19 nm in steps of 3 nm. These six independent runs allow us to verify the convergence of the simulations regardless of whether the CO₂ molecule was initially placed within the polymer region or the bulk water region. Finally, to initialize the simulations, 100 steps of energy minimization with the steepest descent algorithm were used, before MD simulations were run for

36 ns with a time step of 1 fs.

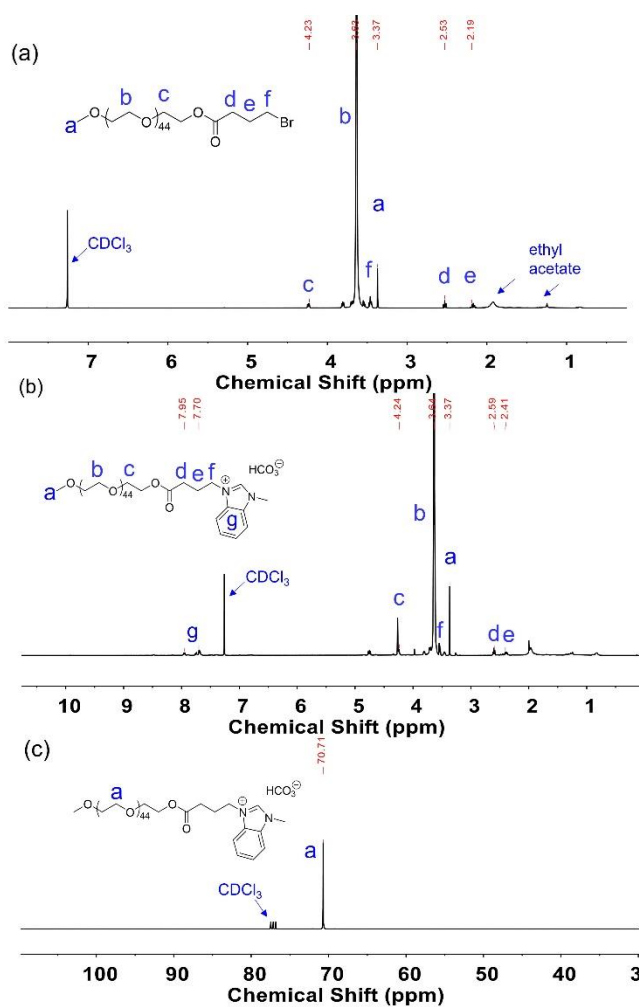


Figure S1. ¹H NMR spectra of (a) halide end polymer PEO₄₄-Br and (b) methylbenzimidazolium-terminated polymer PEO₄₄-Im (P1) with (c) ¹³C NMR spectra.

Br-terminated poly(ethylene oxide) (PEO₄₄-Br) was synthesized through the dicyclohexylcarbodiimide (DCC) coupling reaction between PEO₄₄-OH and 4-bromobutyric acid. After purified by precipitating into cold diethyl ether for three times, the powder was collected and ready for use later. ¹H NMR (400 MHz, CDCl₃) δ (ppm): a: -CH₃ 3.37, b: PEO 3.63, c: -CH₂- 4.23, d: -CH₂- 2.53, e: -CH₂- 2.19. Subsequently, the halide ended PEO₄₄-Br was converted through alkylation with 1-methylbenzimidazole in DMF at 95 °C for 24 h in the atmosphere of N₂. The powder of PEO₄₄-Im was obtained after precipitating in diethyl ether. Finally, the anion exchange was carried out through the reaction with KHCO₃. ¹H NMR (400 MHz, CDCl₃) δ (ppm): a: -CH₃ 3.37, b: PEO 3.64, c: -CH₂- 4.24, d: -CH₂- 2.59, e: -CH₂- 2.41, g: aromatic 7.95~7.70. Besides, the ¹³C NMR (400 MHz, CDCl₃) spectra of P1 also shows the characteristic peaks of PEO at 70.71 ppm.

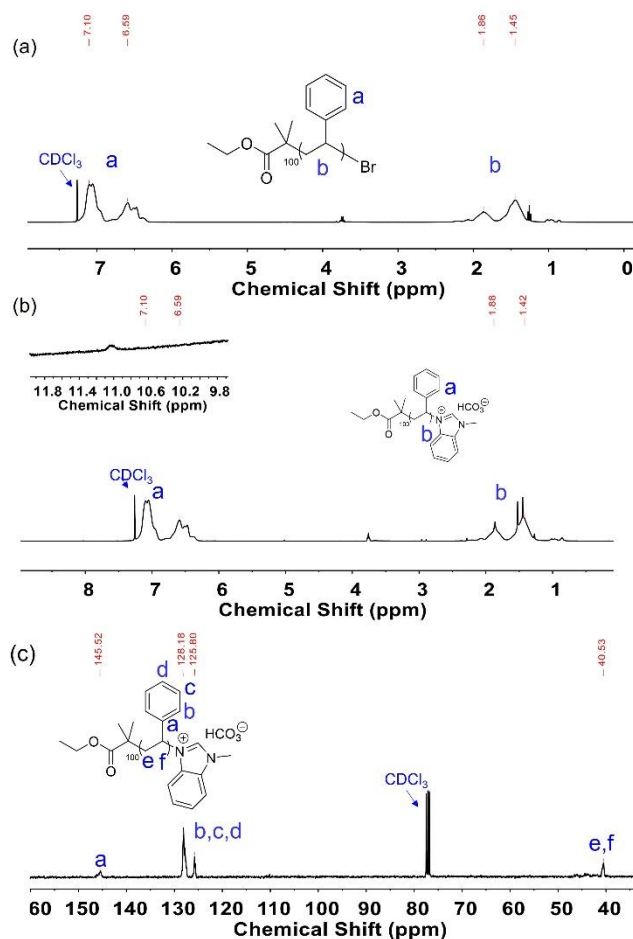


Figure S2. ^1H NMR spectra of (a) halide end polymer $\text{PS}_{100}\text{-Br}$ and (b) methylbenzimidazolium-terminated polymer $\text{PS}_{100}\text{-Im}$ (P2) with (c) ^{13}C NMR spectra.

$\text{PS}_{100}\text{-Br}$ was synthesized using ethyl α -bromoisobutyrate (EBiB) as an initiator through atom transfer radical polymerization (ATRP) in anisole at 90°C for 12 h. After precipitation with methanol, the polymer powder was collected and dried under vacuum. The number of repeat units of styrene was calculated to be 100 through end-group analysis using ^1H NMR peak at 4.4 ppm of the $-\text{CH}-$ end group directly connected with Br atom in $\text{PS}\text{-Br}$. ^1H NMR (400 MHz, CDCl_3) δ (ppm): a: aromatic 7.10~6.59, b: $-\text{CH}_2\text{-CH}-$ 1.86~1.45. Subsequently, end group functionalization was used to synthesize the $\text{PS}_{100}\text{-Im}$ through the quaternization reaction between $\text{PS}\text{-Br}$ and 1-methylbenzimidazole at 95°C for 24 h in DMF. ^1H NMR (400 MHz, CDCl_3) δ (ppm): a: aromatic 7.10~6.59, b: $-\text{CH}_2\text{-CH}-$ 1.88~1.42. The peak at 11.1 ppm could be assigned to the proton in $N\text{-CH-N}$ indicating the successful reaction of the ended $-\text{Br}$ group. Besides, ^{13}C NMR spectra of P2 in CDCl_3 was also characterized which showing peaks of benzene ring (a,b,c,d) and $-\text{CH}_2\text{-CH}-$ (e,f) (Figure S2c).

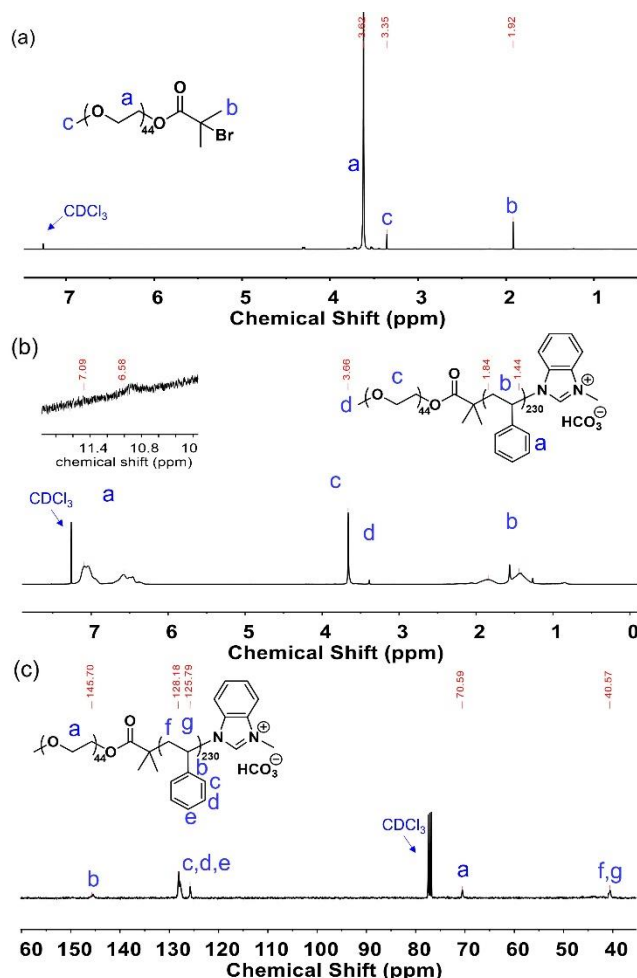


Figure S3. ¹H NMR spectra of (a) PEO₄₄-Br ATRP macroinitiator, (b) methylbenzimidazolium-terminated polymer PEO₄₄-b-PS₂₃₀-Im (P3) with (c) ¹³C NMR spectra.

The ATRP initiator PEO₄₄-Br was synthesized between PEO₄₄-OH and α -bromoisobutyl bromide under room temperature for 36 h. After precipitation with cold diethyl ether, the prepared initiator was collected for use later. ¹H NMR (400 MHz, CDCl₃) δ (ppm): a: PEO 3.62, b: -C₂H₆ 1.92, c: -CH₃ 3.35. PEO₄₄-b-PS₂₃₀-Br was synthesized using prepared PEO₄₄-Br as a macroinitiator reacted with styrene in anisole at 90 °C for 12 h through ATRP. After precipitation with cooled n-hexane three times and dried under vacuum, the prepared BCP was obtained. Likewise, the reaction between KHCO₃ and PEO₄₄-b-PS₂₃₀-Im was carried out for the anion exchange process. ¹H NMR (400 MHz, CDCl₃) δ (ppm): a: aromatic 7.09~6.58, b: -CH₂-CH- 1.84~1.44, c: PEO 3.66. Notably, peak at 11.1 ppm representing the proton in *N*-CH-*N* indicates the successful reaction of the ended -Br group. In addition, ¹³C NMR spectra of P3 in CDCl₃ shows the characteristic peaks of benzene ring (b,c,d,e), -CH₂-CH- (f,g) and PEO (a)(Figure S3c).

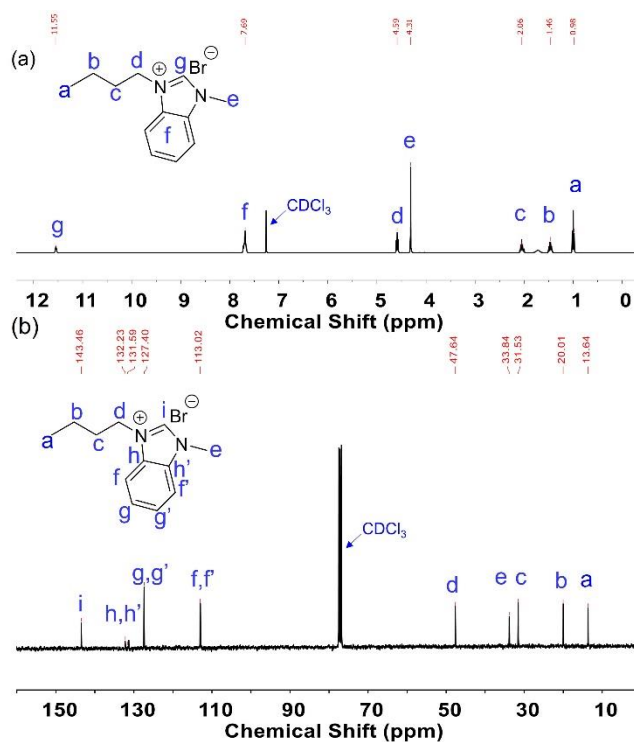


Figure S4. (a) ¹H NMR spectra and ¹³C NMR spectra of 1-butyl-3-methyl-1H-benzimidazolium.

BMB-Im was synthesized between N-methyl benzimidazole and 1-bromobutane in acetonitrile at 85 °C overnight. After wash with hexane several times, the final product was obtained. ¹H NMR (400 MHz, CDCl₃) δ (ppm): a: 0.98, b: 1.46, c: 2.06, d: 4.59, e: 4.31, f: 7.69, g: 11.55. Besides, ¹³C NMR spectra in CDCl₃ also shows characteristic peaks of BMB-Im including benzene ring (f,g,h) and proton in *N*-CH-*N* which consist with those in polymer NHC ligands.

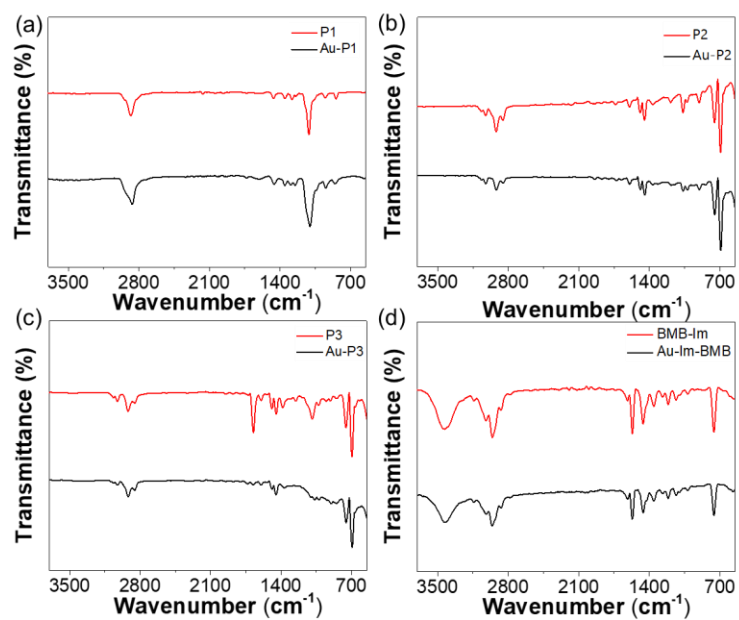


Figure S5. FT-IR spectra of pure ligands (a) P1 and Au NPs modified by P1, (b) P2 and Au NPs modified by P2, (c) P3 and Au NPs modified by P3 and (d) BMB-Im and Au NPs modified by BMB-Im.

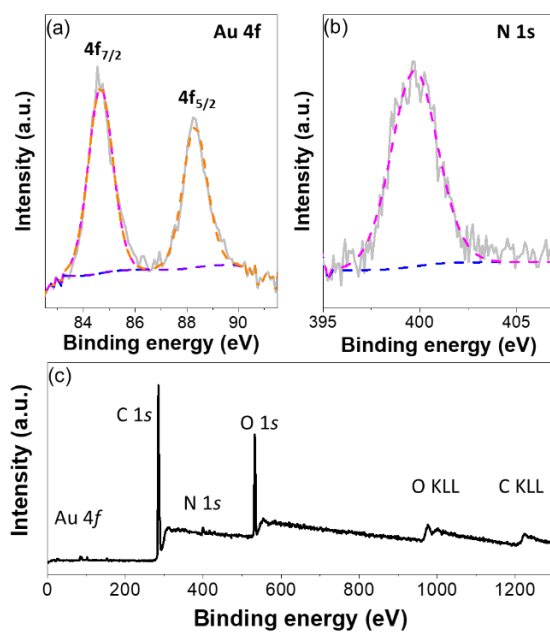


Figure S6. High resolution XPS spectra of (a) Au 4f, (b) N 1s and survey spectra (c) of BMB-Im modified Au/C samples.

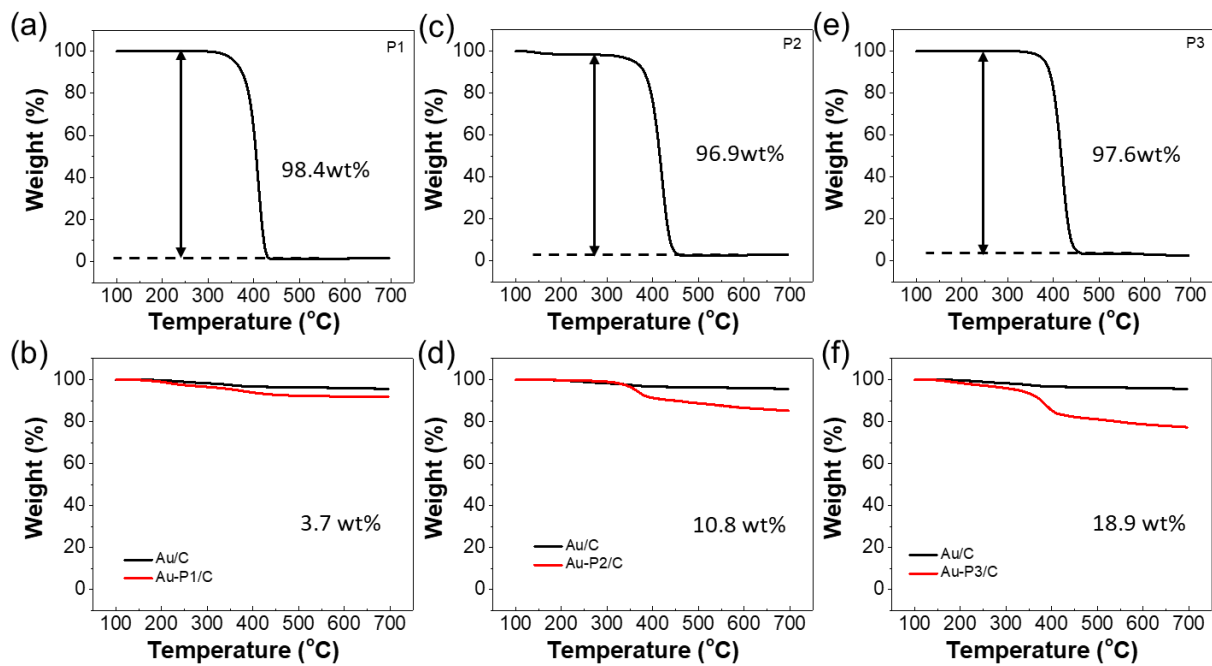


Figure S7. TGA curves of (a, b) P1, Au/C and Au-P1/C, (c, d) P2, Au/C and Au-P2/C and (e, f) P3, Au/C and Au-P3/C.

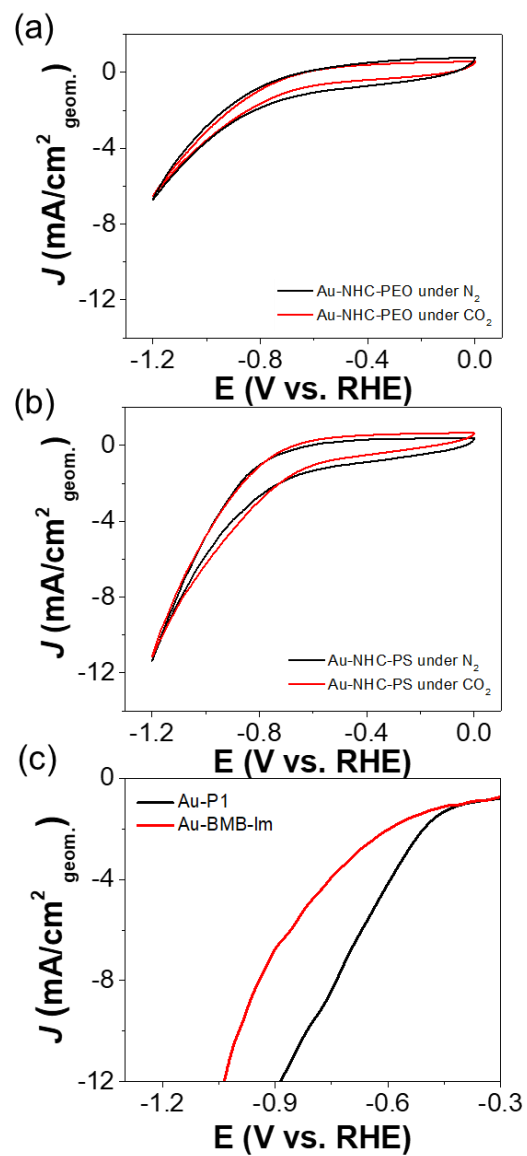


Figure S8. CV curves of Au-P1 (a), Au-P3 (b) under N₂ (black) and CO₂ (red) and (c) LSV curves of Au-P1 and Au-BMB-Im in 0.1 M KHCO₃ electrolyte.

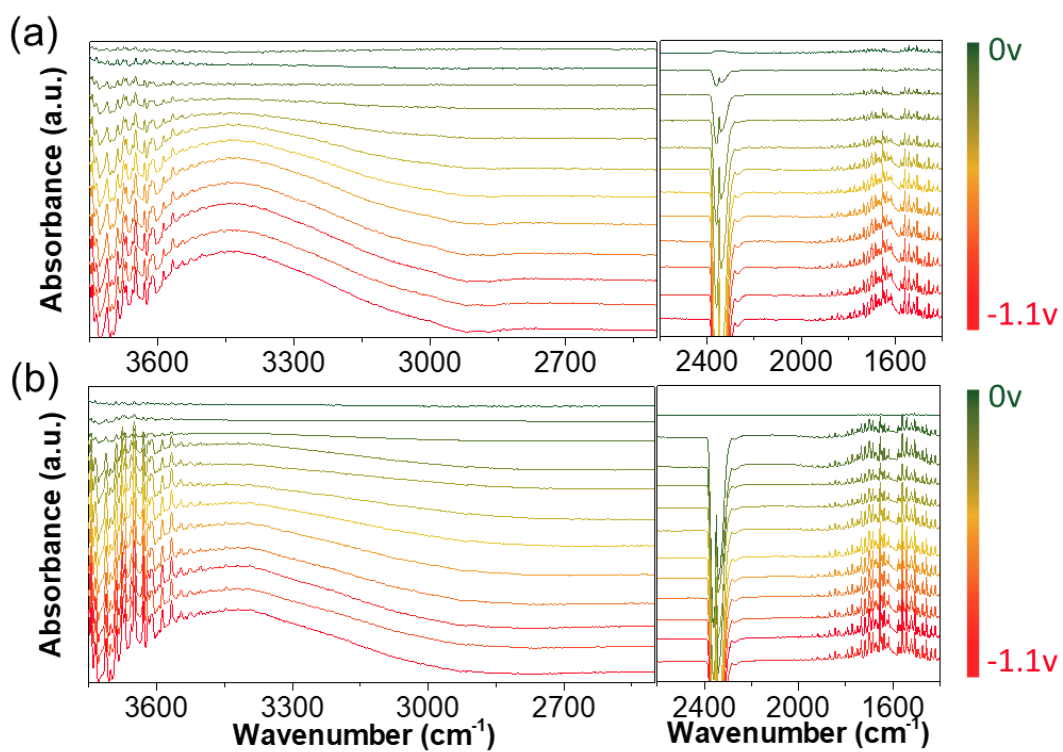


Figure S9. In situ ATR-SEIRAS spectra of (a) Au-P1, (b) Au-BMB-Im in CO_2 purged 0.1 M KHCO_3 with various reductive potentials.

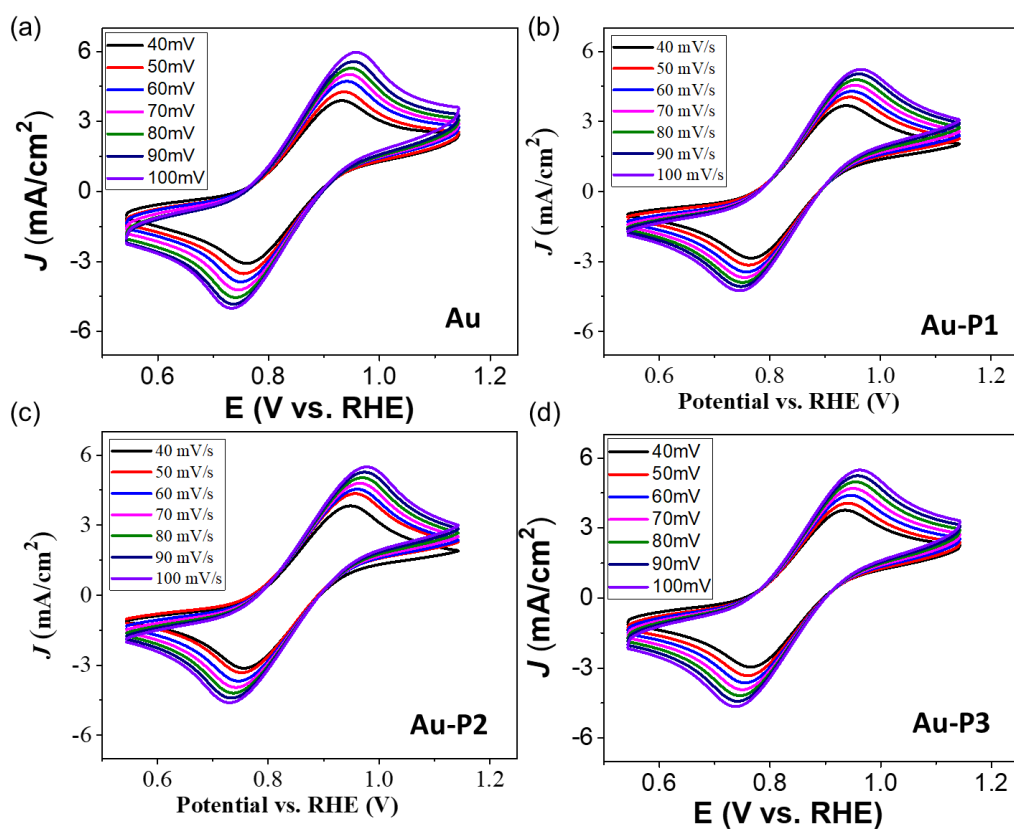


Figure S10. CV curves of pure Au (a), Au-P1 (b), Au-P2 (c) and Au-P3 in the range of 0.5 to 1.1 V with the scan rate from 40 to 100 mV s⁻¹ using K₃Fe(CN)₆ as probe.

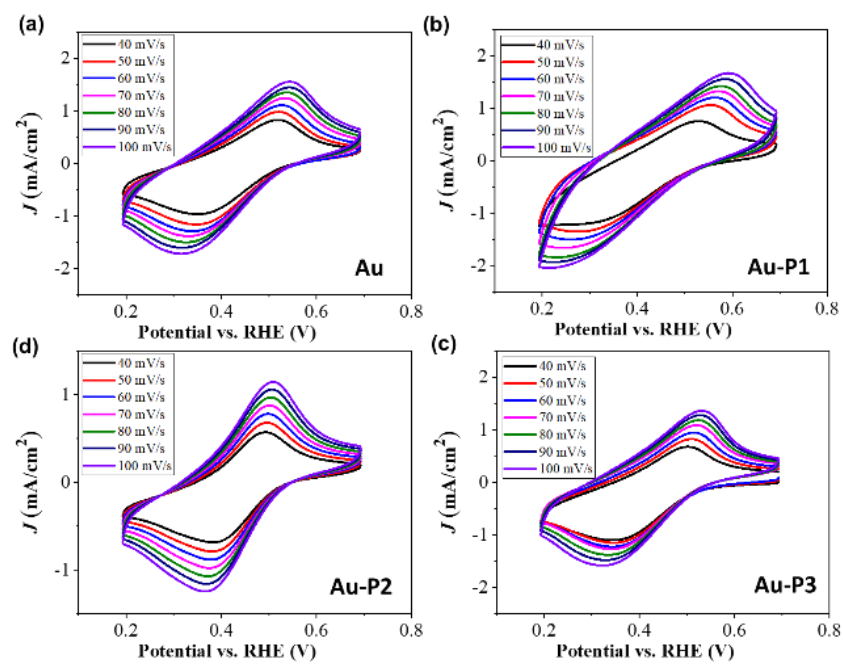


Figure S11. CV curves of pure Au (a), Au-P1 (b), Au-P2 (c) and Au-P3 in the range of 0.5 to 1.1 V with the scan rate from 40 to 100 mV s⁻¹ using Ru(NH₃)₆Cl₃ as probe.

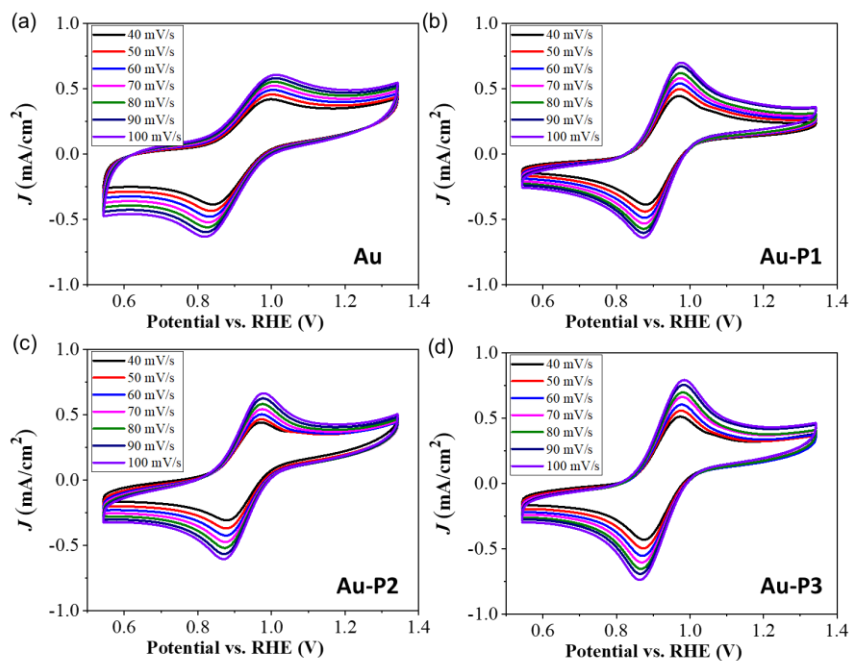


Figure S12. CV curves of pure Au (a), Au-P1 (b), Au-P2 (c) and Au-P3 in the range of 0.5 to 1.1 V with the scan rate from 40 to 100 mV s^{-1} using Fc-COOH as probe.

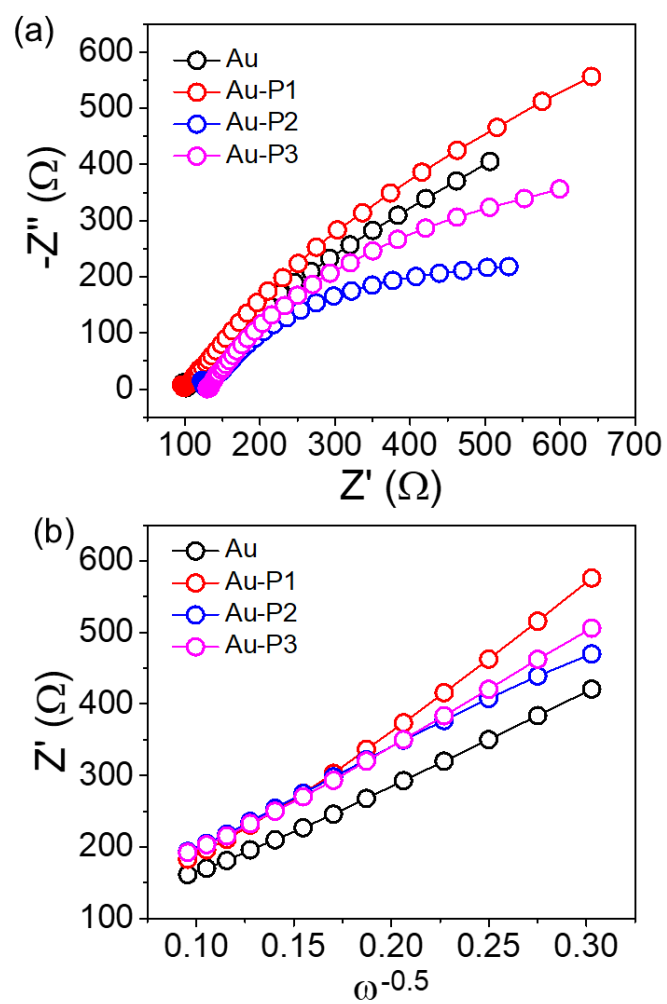


Figure S13. (a) The EIS plots and (b) corresponding Z' against $\omega^{-0.5}$ of pure Au and Au modified with various ligands including P1, P2 and P3.

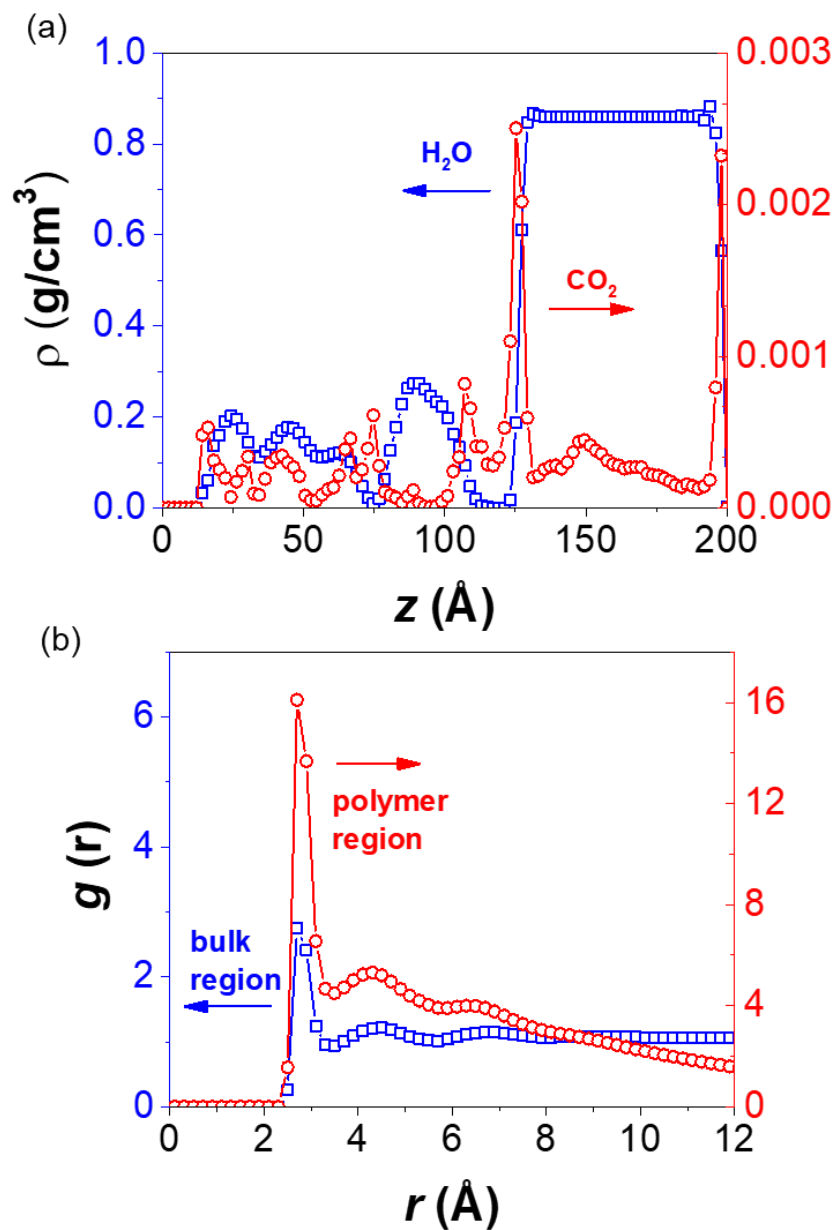


Figure S14. (a) Density profiles as a function of z coordinates, with water and CO₂ shown in blue and red when one CO₂ molecule was incorporated into the system; (b) Ow-Ow radial distribution function, analyzed for water molecules above $z = 11.8$ nm (bulk region, blue) and those below $z = 11.8$ nm (polymer layer, red).

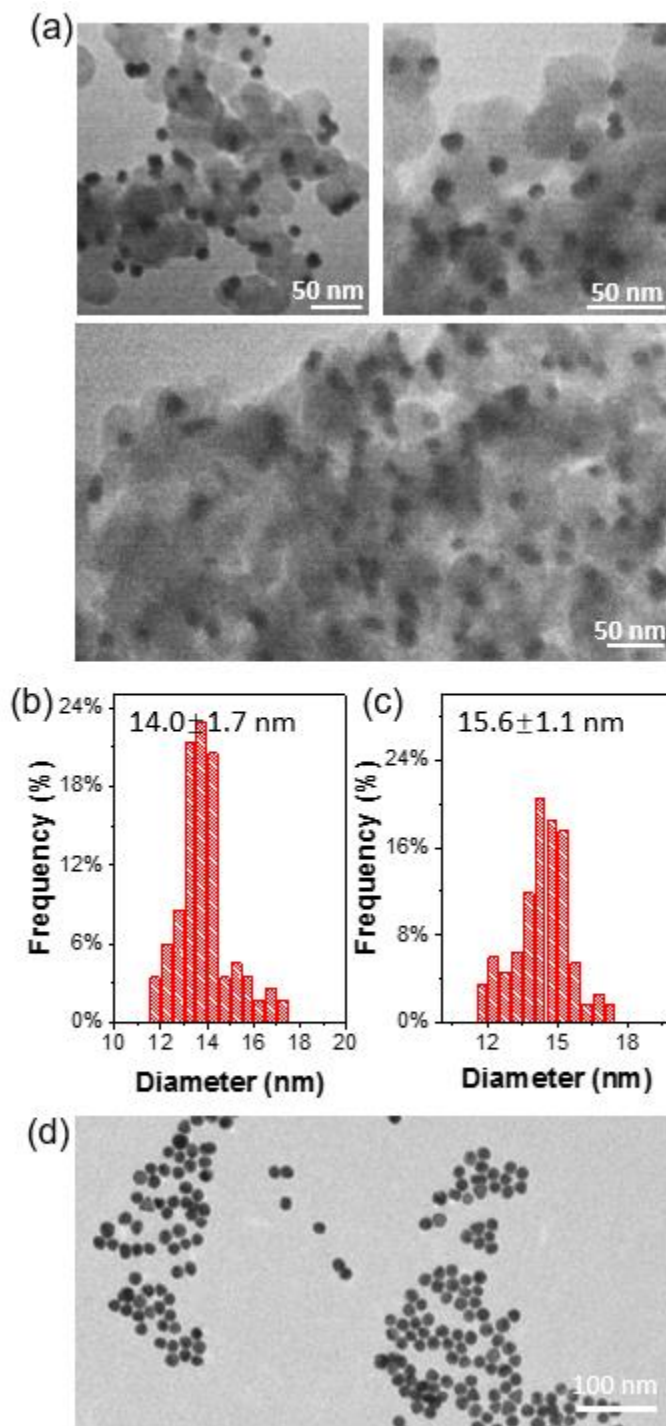


Figure S15. (a) Additional TEM images for AuNPs capped by P3 after electrolysis for 1 h at -1.0V and size distribution of AuNPs (b) before and (c) after electrolysis. (d) TEM image of as-synthesized AuNPs.

Table S1. Faradic efficiency and partial current density analysis data of pure Au catalysts.

Potential (V vs RHE)	F.E. of CO (%)			Average (%)	Standard Deviation	CO/H ₂
-0.7	72.1	66.4	71.8	70.1	2.6	2.4
-0.8	68.1	73.7	71.8	71.2	2.3	2.5
-0.9	74.2	76.1	77.1	75.8	1.2	3.1
-1	65.2	67.1	72.3	68.2	3.0	2.2
-1.1	63.2	61.2	66.9	63.8	2.4	1.8

Potential (V vs RHE)	F.E. of H ₂ (%)			Average (%)	Standard Deviation	CO/H ₂
-0.7	27.6	34.2	26.5	29.4	3.4	2.4
-0.8	26.6	30.2	29.6	28.8	1.6	2.5
-0.9	24.6	23.2	25.1	24.3	0.8	3.1
-1	34.2	31.9	27.3	31.1	2.9	2.2
-1.1	36.2	38.2	33.2	35.9	2.1	1.8

Potential (V vs RHE)	j_{total} (mA cm ⁻²)	j_{CO} (mA cm ⁻²)	Standard Deviation	j_{H_2} (mA cm ⁻²)	Standard Deviation	j_{CO}/j_{H_2}
-0.7	-4.7	-3.3	0.1	-1.4	0.2	2.4
-0.8	-6.9	-4.9	0.2	-2.0	0.1	2.5
-0.9	-9.4	-7.2	0.1	-2.3	0.1	3.1
-1	-13.2	-9.0	0.4	-4.1	0.4	2.2
-1.1	-19.4	-12.4	0.5	-7.0	0.4	1.8

Standard deviations from three independent measurements

Table S2. Faradic efficiency and partial current density analysis data of Au-P1/C catalysts.

Potential (V vs RHE)	F.E. of CO (%)			Average (%)	Standard Deviation	CO/H ₂
-0.7	86.2	84.9	82.5	84.5	1.5	4.7
-0.8	80.4	83.2	85.9	83.2	2.2	5.0
-0.9	87.8	82.4	83.5	84.6	2.3	5.5
-1	71.9	76.2	71.2	73.1	2.2	2.9
-1.1	78.5	80.5	72.8	77.3	3.3	3.9

Potential (V vs RHE)	F.E. of H ₂ (%)			Average (%)	Standard Deviation	CO/H ₂
-0.7	19.0	15.3	19.1	17.8	1.8	4.7
-0.8	17.6	16.7	15.3	16.5	0.9	5.0
-0.9	15.1	15.0	16.4	15.5	0.6	5.5
-1	25.3	24.3	26.2	25.3	0.8	2.9
-1.1	22.1	19.6	18.4	20.0	1.5	3.9

Potential (V vs RHE)	j_{total} (mA cm ⁻²)	j_{CO} (mA cm ⁻²)	Standard Deviation	j_{H_2} (mA cm ⁻²)	Standard Deviation	j_{CO}/j_{H_2}
-0.7	-6.8	-5.8	0.1	-1.2	0.1	4.7
-0.8	-9.6	-8.0	0.2	-1.6	0.1	5.0
-0.9	-12.4	-10.5	0.3	-1.9	0.1	5.5
-1	-16.2	-11.8	0.4	-4.1	0.1	2.9
-1.1	-20.8	-16.1	0.7	-4.2	0.3	3.9

Standard deviations from three independent measurements

Table S3. Faradic efficiency and partial current density analysis data of Au-P2/C catalysts.

Potential (V vs RHE)	F.E. of CO (%)			Average (%)	Standard Deviation	CO/H ₂
-0.7	90.8	89.9	86.2	88.9	2.0	8.1
-0.8	91.7	93.3	85.4	90.1	3.4	8.6
-0.9	89.8	87.1	90.6	89.2	1.5	8.1
-1	82.5	80.9	86.1	83.2	2.2	4.6
-1.1	88.9	89.9	82	86.9	3.5	6.3

Potential (V vs RHE)	F.E. of H ₂ (%)			Average (%)	Standard Deviation	CO/H ₂
-0.7	9.6	9.8	13.6	11	1.8	8.1
-0.8	9.1	7.3	14.9	10.4	3.2	8.6
-0.9	10.3	15.9	6.9	11.0	3.7	8.1
-1	18.1	20.1	15.9	18.0	1.7	4.6
-1.1	11.8	10.4	19.2	13.8	3.9	6.3

Potential (V vs RHE)	j_{total} (mA cm ⁻²)	j_{CO} (mA cm ⁻²)	Standard Deviation	j_{H_2} (mA cm ⁻²)	Standard Deviation	j_{CO}/j_{H_2}
-0.7	-7.5	-6.7	0.2	-0.8	0.1	8.1
-0.8	-10.9	-9.8	0.4	-1.1	0.4	8.6
-0.9	-14.4	-12.8	0.2	-1.6	0.5	8.1
-1	-18.7	-15.6	0.4	-3.4	0.3	4.6
-1.1	-24.4	-21.2	0.8	-3.4	0.9	6.3

Standard deviations from three independent measurements

Table S4. Faradic efficiency and partial current density analysis data of Au-P3/C catalysts.

Potential (V vs RHE)	F.E. of CO (%)			Average (%)	Standard Deviation	CO/H ₂
-0.7	91.2	85.8	87.1	88.0	2.3	7.3
-0.8	94.8	96.7	89.7	93.7	3.0	11.8
-0.9	93.5	90.5	86.6	90.2	2.8	8.5
-1	88.1	86.1	91.5	88.6	2.2	7.9
-1.1	88.7	81.1	87.7	85.8	3.3	5.5

Potential (V vs RHE)	F.E. of H ₂ (%)			Average (%)	Standard Deviation	CO/H ₂
-0.7	8.9	14.3	12.9	12.0	2.3	7.3
-0.8	7.9	4.5	11.5	8.0	2.9	11.8
-0.9	6.8	11.2	13.9	10.6	2.9	8.5
-1	12.4	15.2	6.1	11.2	3.8	7.9
-1.1	12.1	20.2	14.1	15.5	3.4	5.5

Potential (V vs RHE)	j_{total} (mA cm ⁻²)	j_{CO} (mA cm ⁻²)	Standard Deviation	j_{H_2} (mA cm ⁻²)	Standard Deviation	j_{CO}/j_{H_2}
-0.7	-7.8	-6.9	0.2	-0.9	-0.2	7.3
-0.8	-11.6	-10.9	0.3	-0.9	-0.3	11.8
-0.9	-15.8	-14.2	0.4	-1.7	-0.5	8.5
-1	-20.4	-18.1	0.5	-2.3	-0.8	7.9
-1.1	-25.8	-22.1	0.9	-4.0	-0.9	5.5

Standard deviations from three independent measurements

References cited in SI

1. W. Li, C.-H. Kuo, I. Kanyo, S. Thanneeru and J. He, *Macromolecules*, 2014, **47**, 5932-5941.
2. B. Liu, C.-H. Kuo, J. Chen, Z. Luo, S. Thanneeru, W. Li, W. Song, S. Biswas, S. L. Suib and J. He, *Angewandte Chemie International Edition*, 2015, **54**, 9061-9065.
3. J. He, Y. Liu, T. Babu, Z. Wei and Z. Nie, *Journal of the American Chemical Society*, 2012, **134**, 11342-11345.
4. M. Dunwell, Y. Yan and B. Xu, *Surface Science*, 2016, **650**, 51-56.
5. A. Sukeri, L. P. H. Saravia and M. Bertotti, *Physical Chemistry Chemical Physics*, 2015, **17**, 28510-28514.
6. M. J. Rodríguez Presa, L. M. Gassa, O. Azzaroni and C. A. Gervasi, *Analytical Chemistry*, 2009, **81**, 7936-7943.
7. S. Li, Q. Xu, E. Uchaker, X. Cao and G. Cao, *CrystEngComm*, 2016, **18**, 2532-2540.
8. A. P. Thompson, H. M. Aktulga, R. Berger, D. S. Bolintineanu, W. M. Brown, P. S. Crozier, P. J. in 't Veld, A. Kohlmeyer, S. G. Moore, T. D. Nguyen, R. Shan, M. J. Stevens, J. Tranchida, C. Trott and S. J. Plimpton, *Computer Physics Communications*, 2022, **271**, 108171.
9. M. G. Martin and J. I. Siepmann, *The Journal of Physical Chemistry B*, 1999, **103**, 4508-4517.
10. C. D. Wick, M. G. Martin and J. I. Siepmann, *The Journal of Physical Chemistry B*, 2000, **104**, 8008-8016.
11. C. D. Wick, J. M. Stubbs, N. Rai and J. I. Siepmann, *The Journal of Physical Chemistry B*, 2005, **109**, 18974-18982.
12. N. Rai and J. I. Siepmann, *The Journal of Physical Chemistry B*, 2007, **111**, 10790-10799.
13. S. J. Weiner, P. A. Kollman, D. A. Case, U. C. Singh, C. Ghio, G. Alagona, S. Profeta and P. Weiner, *Journal of the American Chemical Society*, 1984, **106**, 765-784.
14. S. J. Weiner, P. A. Kollman, D. T. Nguyen and D. A. Case, *Journal of Computational Chemistry*, 1986, **7**, 230-252.
15. A. K. Rappe, C. J. Casewit, K. S. Colwell, W. A. Goddard, III and W. M. Skiff, *Journal of the American Chemical Society*, 1992, **114**, 10024-10035.
16. A. Nayis, K. Liebl, C. V. Frost and M. Zacharias, *Biophysical Journal*, 2021, **120**, 101-108.
17. W. L. Jorgensen, J. Chandrasekhar, J. D. Madura, R. W. Impey and M. L. Klein, *The Journal of Chemical Physics*, 1983, **79**, 926-935.
18. J.-P. Ryckaert, G. Ciccotti and H. J. C. Berendsen, *Journal of Computational Physics*, 1977, **23**, 327-341.
19. J. J. Potoff and J. I. Siepmann, *AIChE Journal*, 2001, **47**, 1676-1682.
20. A. V. Marenich, S. V. Jerome, C. J. Cramer and D. G. Truhlar, *Journal of Chemical Theory and Computation*, 2012, **8**, 527-541.